Report

Mathematical Modeling of breast cancer cells in response to endocrine therapy and Cdk4/6 inhibition

Andrea Tonina and Gloria Lugoboni

January 2024

Contents

1 Introduction

1.1 Breast Cancer - General overview

Breast cancer is one of the most common cancer types in this generation. Circa one woman over 8 can be affected by it during her life, indeed, it is the tumor with the highest incidence in women, surpassing lung cancer [1]. Breast cancer is characterized by four stages from the lowest to highest severity and each stage is associated with a specific probability of survival. At stage four metastases usually form, and since only certain organs are attacked, specifically lungs, bones, liver, and brain, we talk of organotropism [2].
Breast cancer can be stratified based on the mRNA expression of 50 genes, a multi-gene signature known as PAM50 which is used to stratify and define risk and biological information of the patients [3]. There are five main subtypes based on PAM50 classification, in this paper we will talk about Luminal A and Luminal B tumors in which the status of the hormone estrogen receptor (ER) is positive, meaning that the tumor cells can grow by using this hormone. Luminal B tumors are more aggressive and usually associated with worse prognosis compared to Luminal A tumors, nevertheless, the five-year survival rate is above 90% in both cases [4].

1.2 Epidemiology of Breast cancer

Globally, the incidence of breast cancer has been rising with an annual increase of 3.1% with a start of 641.000 cases in 1980, and an increase to more than 1.6 million in 2010 [5] and the trend is likely to continue. In the last decade, clinical treatments evolved mainly considering that breast cancer is a molecularly heterogeneous disease. The classification proposed by Perou and Sorlie in 2000 stratifies the breast cancer disease into four molecular subtypes: luminal A and luminal B which express estrogen receptor (ER), basal-like and human epidermal growth factor receptor 2 (HER2, encoded by ERBB2) characterized by a lack of ER expression [6]. Breast cancer expressing estrogen receptor and/or progesterone receptor (PR) is considered hormone receptor-positive breast cancer, where tumors that don't express ER, PR or HER2 are classified as triple-negative breast cancer (TNBC)[7].

Different subtypes lead to different death rates, with HER2 subtypes showing a higher rate of death, followed by the TNBC, luminal A, and luminal B subtypes [8]. Moreover, the incidence of tumor subtypes varies by ethnicity, for example, African-American women have the highest rate of TNBC compared with any other ethnic groups and they also show higher rates of metastatic disease which is associated with a lower survival rate [9]. Even though it varies by ethnicity, across countries, and molecular subtypes, approximately 10% of all breast cancers are inherited and associated with family history [10]. Indeed, evidence suggests that individuals with first-degree relatives who had breast cancer have an elevated relative risk of early-onset breast cancer[11].

Table makes an overview on breast cancer molecular subtypes:

BRCA molecular subtypes	Hormone receptors	HER2	Annotations
Luminal A	+	-	Low-grade, tend to grow slowly and have the best prognosis
Normal-like	+	-	Slightly worse prognosis than luminal A
Luminal B	+	+	Grow slightly faster than Luminal A cancers
	+	-	and prognosis is slightly worse
Triple-negative	-	+	More common in women with BRCA1 mutations
HER2-enriched (non luminal)	-	+	Grow faster than luminal cancers and have worse prognosis

1.3 Endocrine therapies and Cdk4/6 inhibition

1.3.1 Cyclin-dependent kinases Cdk4/6 and Palbociclib

CDK4 and CDK6, two proteins known as cyclin-dependent kinases, play a crucial role in the transition of cells from the G1 phase to the S phase of the cell cycle. They are essential for the initiation, growth, and survival of many types of cancer [12].

Palbociclib is an orally available inhibitor of both CDK4 and CDK6-cyclinD1 kinase activity and is used to treat hormone receptor-positive (HR+) and HER2-negative breast cancer. Palbociclib was the first CDK4/6 inhibitor to

be approved as a cancer therapy. In the G1 phase of the cell cycle, mammalian cells must pass a checkpoint, known as the restriction point "R", to complete the cell cycle and divide. Regulation of one or more proteins involved in this checkpoint is lost in many cancers. However, by inhibiting CDK4/6, palbociclib prevents the cell from passing R and exiting G1, and in turn from proceeding through the cell cycle [13].

1.3.2 Endocrine therapies

ER+ tumors are characterized by the presence of the estrogen receptor on the surface of tumor cells. These receptors are activated by 17 β-oestradiol (referred to as E2), one of the major endogenous estrogens. Once the receptor is bound by E2, a signaling process is activated, enhancing transcriptional processes and signaling events that result in the control of gene expression, such as the ones allowing cell cycle progression [14].
There are several types of endocrine therapy (also known as hormone therapy) for breast cancer. These therapies aim to lower E2 levels in the body and prevent E2 from binding to the estrogen receptor.

- **Selective estrogen receptor modulators (SERMs)**. These drugs have an antagonist activity thanks to which they can interact with the estrogen receptor preventing the binding with E2 and therefore, preventing the receptor activation [14].
- **Selective estrogen receptor degraders or downregulators (SERDs)**. The mechanism of action of these drugs is similar to the one of SERMs. In this case, SERDs bind to the estrogen receptor and activate a process of degradation that causes a downregulation of the signaling. One example is Fulvestrant, also known as ICI 182,780. It is been used for over 10 years, specifically as a treatment of advanced breast cancer in both pre and postmenopausal women [15].
- **Lower estrogen levels**. In this case, the idea is to reduce the level of estrogen, therefore slowing cancer growth. An example is aromatase inhibitors (AIs) which corresponds to a class of drugs that can block the enzyme aromatase, which is the enzyme able to synthetase estrogen [16].

2 Material and Methods

2.1 Cell culture and treatments

MCF-7 is a human breast cancer cell line positive for the estrogen receptor [17], which was used to define and study the breast cancer model. The cell culture was followed for 7 days and during this time frame the research group measured the level of key proteins and proliferation markers to assess changes in the cancer cells and observe their behavior when treated. Specifically, the research group combined endocrine therapies and Cdk4/6 inhibition, this was achieved using the following drugs:

- Fulvestrant, a selective estrogen receptor degrader (SERD).
- Palbociclib, a Cdk4/6 inhibitor.

MCF-7 cells are ER+, which means that their growth depends on the presence of E2, and knowing that the research group was able to lower the estrogen levels by modulating the quantity of 17 beta-Estradiol in the growth medium. MCF-7 cells present an internal concentration of E2 that is considered aberrant. Due to this, the absence of E2 in the medium is still not sufficient to bring the internal concentration of E2 to 0, rather it decreases over time till a minimum amount. In the presence of an environment without E2, the cells can change the composition of the medium by generating an E2 level that enables the maintenance of their proliferation. For this reason, once modeling E2 deprivation, two parameters are considered, one regarding the concentration of E2 in the medium and one to account for the decreasing of internal E2 concentration.
The treatment medium (Fulvestrant/Palbociclib -E2) was added to the cells at day 0 and day 3.

2.2 Model structure

Figure 1 represents the interactions between the key proteins regulating the signaling and proliferation processes given by the presence of E2.
In the presence of E2, ER is bound (biological process (1) in Figure 1), and the production of cyclinD1 and c-Myc is amplified (biological process (3) and (4)), where the first is a protein required to have a progression in the cell cycle [19], while the second is a transcription factor able to activate the expression of pro-proliferative genes [20].

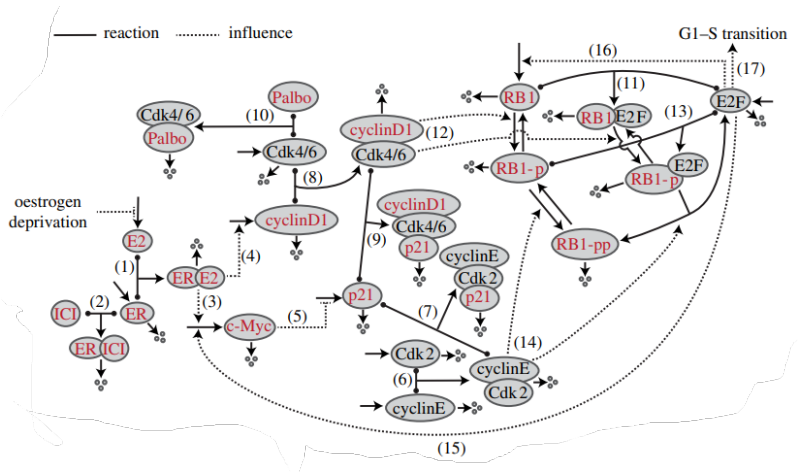

Figure 1: From [18]. Visual representation of the biological mechanism. Solid lines with dots represent reversible binding reactions, other solid lines represent the production or degradation of proteins, dashed lines represent influences with arrowheads representing enhancement and blunt heads representing inhibition. The numbers between parenthesis represent a specific biological process.

CyclinD1 acts combined with Cdk4/6 to hypophosphorylate RB1, obtaining RB1-p (biological process (8) and (12)). In its hypophosphorylated state, RB1 can bind the transcription factor E2F (biological process (13)), inhibiting cell cycle progression and differentiation [21].

CyclinE once combined with Cdk2 can hyperphosphorylate RB1-p obtaining RB1-pp (biological process (6) and (14)). In this state, RB1 is no longer capable of binding and inhibiting E2F, therefore allowing the transition to phase S and cell proliferation [21] (biological process (15), (16) and (17)).

p21 and p27 are CDK inhibitors, they can inactivate the complexes cyclinD1:Cdk4/6 and cyclinE:Cdk2 [22] (biological process (7)). Despite this, these proteins are inhibited by the production of c-Myc, therefore allowing an enhancement in cell proliferation (biological process (5) and (9)).

In the presence of ICI (Fulvestrant), the degradation of ER is activated, as can be observed in Figure 1 biological process (2). A similar inhibitory activity can be observed in biological processes (10) where palbociclib binds to Cdk4/6 and inactivates it.

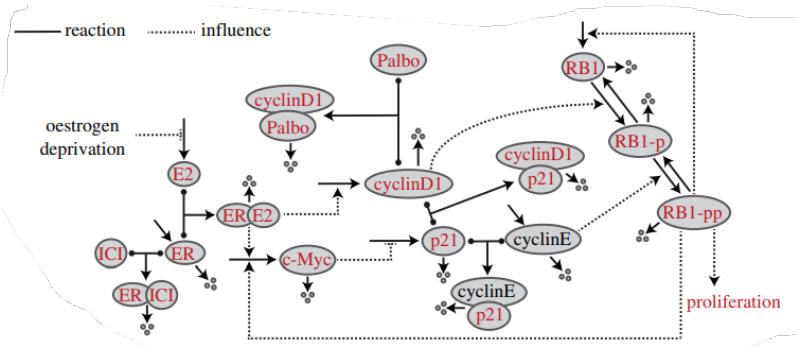

Figure 2: From [18]. Visual representation of the simplified biological process used for the model creation. The species in red were measured by experiment and those in black were not. For p21, cyclinD1 and RB1, the total protein was measured. In addition, RB1-pp was measured.

This complex model can be simplified by reducing the number of species in play, as can be seen in Figure 2, which depicts the final representation that is used to create the mathematical model.

The main simplifications are explained under:

- (a) Cdk4/6 was not modeled explicitly but implicitly, since the researchers considered that all cyclinD1 not bounded to p21 is bound to Cdk4/6 and is therefore in an active form.
  For this reason, the presence of palbociclib, which can inactivate the complex cyclinD1:Cdk4/6, is modeled as bound to cyclinD1.

- (b) Cdk2, as Cdk4/6, is modeled implicitly.
- (c) E2F is not modeled, it's transcriptional activity is considered proportional to the quantity of RB1-pp present. Even though this approximation could seem too much from a biological perspective, the obtained results fit perfectly the experimental data.

2.3 Model equation

A more detailed explanation of the parameters found in the following equations can be found in Appendix - B 7.

Equation 1

$$\frac{dER}{dt} = k_{ER} - kd_{ER} \times ER \quad (1)$$

$$-kb_{E2ER} \times E2 \times ER + kub_{E2ER} \times E2ER \quad (2)$$

$$-kb_{ICIER} \times ICI \times ER + kub_{ICIER} \times ICIER \quad (3)$$

(1) Translation and degradation of ER α
(2) Binding and unbinding between ERα and E2
(3) Binding and unbinding between ER α and ICI 182,780

Equation 2

$$\frac{dE2ER}{dt} = -k_{E2ER} \times E2ER \quad (4)$$

$$+kb_{E2ER} \times E2 \times ER + kub_{E2ER} \times E2ER \quad (2)$$

(4) Degradation of E2:ER
(5) Binding and unbinding between ER α and E2

Equation 3

$$\frac{dICIER}{dt} = kb_{ICIER} \times ICI \times ER - kub_{ICIER} \times ICIER \quad (6)$$

$$-kd_{ICIER} \times ICIER \quad (7)$$

(6) Binding and unbinding between ICI 182,780 and ER α
(7) Degradation of ICIER

Equation 4

$$\frac{dcyclinD1}{dt} = -kd_{cyclinD1} \times cyclinD1 \quad (8)$$

$$+k_{cyclinD1} \times \left(1 + k_{cyclinD1E2ER} \times \frac{E2ER^{p_{cyclinD1E2ER_2}}}{p_{cyclinD1E2ER_1}^{p_{cyclinD1E2ER_2}} + E2ER^{p_{cyclinD1E2ER_2}}}\right) \quad (9)$$

$$-kb_{cyclinD1p21} \times cyclinD1 \times p21 + kub_{cyclinD1p21} \times cyclinD1p21 \quad (10)$$

$$-kb_{cyclinD1palbo} \times cyclinD1 \times palbo + kub_{cyclinD1pabo} \times cyclinD1palbo \quad (11)$$

(8) Degradation of cyclinD1
(9) Basal translation of cyclinD1 and the increased translation by E2:ER
(10) Binding and unbinding between cyclinD1 and p21
(11) Binding and unbinding between cyclinD1 and palbociclib

Equation 5

$$\frac{dcyclinD1p21}{dt} = -kd_{cyclinD1} \times cyclinD1p21 \quad (12)$$

$$+kb_{cyclinD1p21} \times cyclinD1 \times p21 - kub_{cyclinD1p21} \times cyclinD1p21 \quad (13)$$

(12) Degradation of p21 bound cyclinD1
(13) Binding and unbinding between cyclinD1 and p21

Equation 6

$$\frac{dcyclinD1palbo}{dt} = -kd_{cyclinD1} \times cyclinD1palbo \quad (14)$$

$$+kb_{cyclinD1palbo} \times cyclinD1 \times palbo - kub_{cyclinD1palbo} \times cyclinD1palbo \quad (15)$$

(12) Degradation of palbociclib bound cyclinD1
(13) Binding and unbinding between cyclinD1 and palbociclib

Equation 7

$$\frac{dcMyc}{dt} = -kd_{cMyc} \times cMyc \quad (16)$$

$$+k_{cMyc} \times \big(1 + k_{cMycE2ER} \times \frac{E2ER^{p_{cMycE2ER_2}}}{p_{cMycE2ER_1}^{p_{cMycE2ER_2}} + E2ER^{p_{cMycE2ER_2}}} \quad (17)$$

$$+k_{cMycRB1pp} \times \frac{RB1pp^{p_{cMycRB1pp_2}}}{p_{cMycRB1pp_1}^{p_{cMycRB1pp_2}} + RB1pp^{p_{cMycRB1pp_2}}}\big) \quad (18)$$

(16) Degradation of c-Myc
(17) Basal translation of c-Myc and the increased translation by E2:ER
(18) Increased translation of c-Myc by RB1-pp

Equation 8

$$\frac{dp21}{dt} = -kd_{p21} \times p21 \quad (19)$$

$$+k_{p21} \times \frac{p_{p21cMyc_1}^{p_{p21cMyc_2}}}{p_{p21cMyc_1}^{p_{p21cMyc_2}} + cMyc^{p_{p21cMyc_2}}} \quad (20)$$

$$-kb_{cyclinD1p21} \times cyclinD1 \times p21 + kub_{cyclinD1p21} \times cyclinD1p21 \quad (21)$$

$$-kb_{cyclinEp21} \times cyclinE \times p21 + kub_{cyclinEp21} \times cyclinEp21 \quad (22)$$

(19) Degradation of p21
(20) Basal translation and inhibition of translation by c-Myc
(21) Binding and unbinding between cyclinD1 and p21
(22) Binding and unbinding between cyclinE and p21

Equation 9

$$\frac{dcyclinE}{dt} = k_{cyclinE} - kd_{cyclinE} \times cyclinE \quad (23)$$

$$-kb_{cyclinE} \times cyclinE \times p21 + kub_{cyclinEp21} \times cyclinEp21 \quad (24)$$

(23) Translation and degradation of cyclinE
(24) Binding and unbinding between cyclinE and p21

Equation 10

$$\frac{dcyclinEp21}{dt} = -kd_{cyclinE} \times cyclinEp21 \quad (25)$$

$$+kb_{cyclinEp21} \times cyclinE \times p21 - kub_{cyclinEp21} \times cyclinEp21 \quad (26)$$

(25) Degradation of p21 bound cyclinE
(26) Binding and unbinding between cyclinE and p21

Equation 11

$$\frac{dRB1}{dt} = k_{RB1} - kd_{RB1} \times RB1 \quad (27)$$

$$+k_{RB1RB1pp} \times \frac{RB1pp^{p_{RB1RB1pp_2}}}{p_{RB1RB1pp_1}^{p_{RB1RB1pp_2}} + RB1pp^{p_{RB1RB1pp_2}}} \quad (28)$$

$$-k_{RB1cyclinD1} \times cyclinD1 \times \frac{RB1^{p_{cyclinD1RBrb1_2}}}{p_{cyclinD1RB1_1}^{p_{cyclinD1RB1_2}} + RB1^{p_{cyclinD1RB1_2}}} \quad (29)$$

$$k_{RB1pdepho} \times \frac{RB1p^{p_RB1p_2}}{p_{p_{RB1p_2}} + RB1p^{p_{RB1p_2}}} \quad (30)$$

(27) Degradation of RB1 and basal translation
(28) Increased translation by E2F, modeled as proportional to RB1-pp
(29) Phosphorylation of RB1 by cyclinD1
(30) Dephosphorylation of RB1-p

Equation 12

$$\frac{dRB1p}{dt} = -kd_{RB1p} \times RB1p \quad (31)$$

$$+k_{RB1cyclinD1} \times cyclinD1 \times \frac{RB1^{p_{cyclinD1RB1_2}}}{p_{cyclinD1RB1_1}^{p_{cyclinD1RB1_2}} + RB1^{p_{cyclinD1RB1_2}}} \quad (32)$$

$$-k_{RB1pdepho} \times \frac{RB1p^{p_{RB1p_2}}}{p_{RB1p_1}^{p_{RB1p_2}} + RB1p^{p_{RB1p_2}}} \quad (33)$$

$$-k_{RB1pcyclinE} \times cyclinE \times \frac{RB1p^{p_{cyclinERB1p_2}}}{p_{cyclinERB1p_1}^{p_{cyclinERB1p_2}} + RB1p^{p_{cyclinERB1p_2}}} \quad (34)$$

$$+k_{RB1ppdepho} \times \frac{RB1pp^{p_{RB1pp_2}}}{{p_{RB1pp_1}}^{p_{RB1pp_2}} + RB1pp^{p_{RB1pp_2}}} \quad (35)$$

(31) Degradation of RB1-p
(32) Phosphorylation of RB1 by cyclinD1
(33) Dephosphorylation of RB1-p
(34) Phosphorylation of RB1-p by cyclinE
(35) Dephosphorylation of RB1-pp

Equation 13

$$\frac{dRB1pp}{dt} = -kd_{RB1pp} \times RB1pp \quad (36)$$

$$+k_{RB1pcyclinE} \times cyclinE \times \frac{RB1p^{p_{cyclinERB1p_2}}}{p_{cyclinERB1p_1}^{p_{cyclinERB1p_2}} + RB1p^{p_{cyclinERB1p_2}}} \quad (37)$$

$$-k_{RB1ppdepho} \times \frac{RB1pp^{p_{RB1pp_2}}}{p_{RB1pp_1}^{p_{RB1pp_2}} + RB1pp^{p_{p_{RB1pp_2}}}} \quad (38)$$

(36) Degradation of RB1-pp
(37) Phosphorylation of RB1-p by cyclinE
(38) Dephosphorylation of RB1-pp

Equation 14

$$\frac{dcell}{dt} = k_{pro} \times \left(1 + k_{proRB1pp} \times \frac{RB1pp^{p_{proRB1pp_2}}}{p_{proRB1pp_1}^{p_{proRB1pp_2}} + RB1pp^{p_{proRB1pp_2}}}\right) \times cell \times \left(1 - \frac{cell}{k_{carrying}}\right) \quad (39)$$

(39) Basal proliferation and the increased proliferation by RB1-pp
To model resistance, we added the following equation:

$$\frac{dres}{dt} = par1_{res} \times palbo - par2_{res} \times res \quad (40)$$

and added one term to the cyclinD1 equation:

$$\frac{dcyclinD1}{dt} = -kd_{cyclinD1} \times cyclinD1 \quad (8)$$

$$+k_{cyclinD1} \times \left(1 + k_{cyclinD1E2ER} \times \frac{E2ER^{p_{cyclinD1E2ER_2}}}{p_{cyclinD1E2ER_1}^{p_{cyclinD1E2ER_2}} + E2ER^{p_{cyclinD1E2ER_2}}}\right) \quad (9)$$

$$-kb_{cyclinD1p21} \times cyclinD1 \times p21 + kub_{cyclinD1p21} \times cyclinD1p21 \quad (10)$$

$$-kb_{cyclinD1palbo} \times cyclinD1 \times palbo + kub_{cyclinD1pabo} \times cyclinD1palbo \quad (11)$$

$$+par3_{res} \times \frac{res^{par5_{res}}}{par4_{res}^{par5_{res}} + res^{par5_{res}}} \quad (41)$$

where: $par1_{res} = 1e^{-4}$, $par2_{res} = 1e^{-3}$, $par3_{res} = 0.819$, $par4_{res} = 0.06$, $par5_{res} = 4.87$

2.4 Parameter estimation

Degradation rates were assigned according to what the research group could find in the literature while the other parameters were estimated using MATLAB. Specifically, the parameters were divided into groups associated with each protein of interest (e.g. ER and c-Myc) and a global optimization was performed using the genetic algorithm function *ga* combining it with the refinement function *fminsearch*. The process of optimization was necessary to limit the differences between the simulation and the experimental results.

3 Reimplementation

We decided to implement a simple code in MATLAB that uses an ODE solver to retrieve the main plots that can be found in the original paper. We specifically took as input parameters used and made available by the research group, we also defined the ODEs that are described in section 2.3. No parameter estimation was performed, even though our initial plan was to re-implement the estimation using a gradient-based approach to observe the differences with the estimation effectuated by the group using a genetic algorithm and a refinement function. Cell proliferation estimation was possible by implementing in the code the function retrieved by the group, as will be explained in section 4.3. The experimental values to compare the simulation results were also retrieved from the original paper. We also tried to implement a stochastic version of the code. Specifically, from the ordinary differential equations we tried to infer reaction systems [23] and the deterministic reaction rates (k) were converted into stochastic reaction rates (c), as we saw during the lectures. We generated the stochiometric matrices starting from the obtained reaction system and we finally defined the initial states for the variables as performed in the first implementation (deterministic code). The reactions and the corresponding reaction rates can be found in Appendix - C in section 8). We decided to apply the RSSA approach to simulate the system, we specifically chose this method cause it represents the one that we think could be most efficient for our system, given the number of reactions, and also, is the method that most fascinated us during lectures. Further explanation of the results of this implementation can be found in Appendix - C in Figure 14.

4 Results

4.1 The proposed model structure can largely explain the experimental data

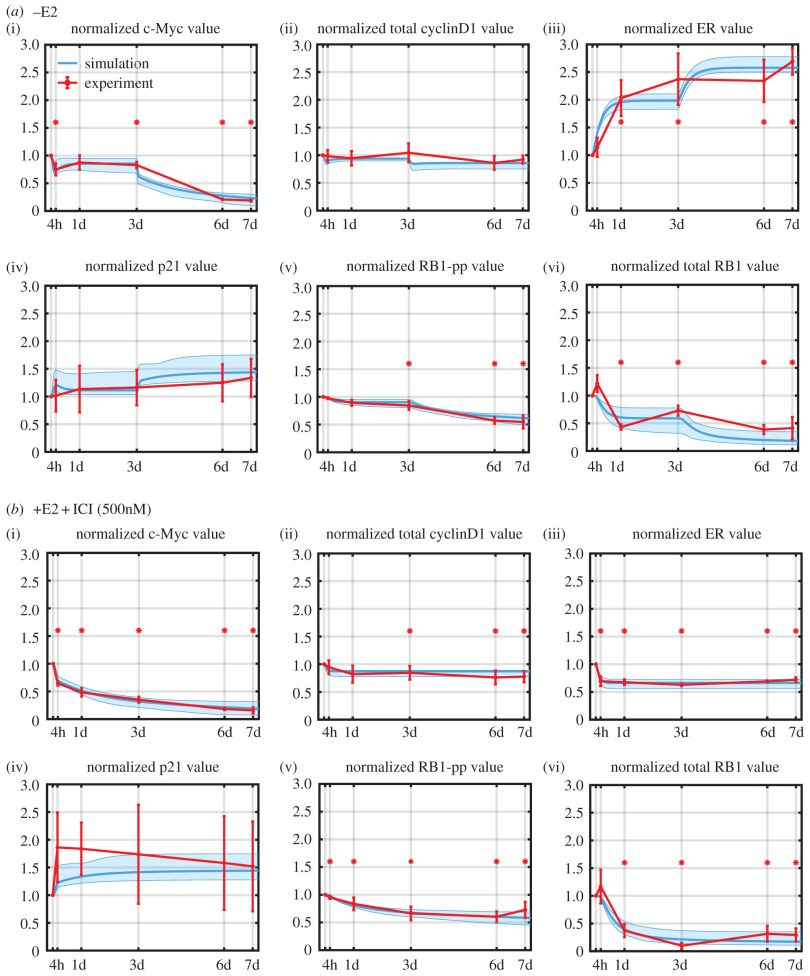

Figure 3: From [18]. Simulation and experimental results for protein-level changes under the different treatment conditions used for model calibration. The experimental measurements are shown in red and the simulation results are shown in cyan (lowest cost simulation as a solid line and the interval containing the central 98% of the cohort simulations as a shaded region). Statistically significant changes are denoted by an asterisk.

The model was calibrated thanks to training data retrieved from time-course measurements of the proteins colored in red in Figure 2. The parameters were estimated by using a genetic algorithm and creating a total of 400 sets of parameters to better calibrate the model. The results of the calibration and estimation can be seen in Figure 3.

Figure 3 (a) depicts protein-level changes after E2 deprivation over 7 days, while Figure 3 (b) depicts protein-level changes after +E2 + ICI treatment over 7 days.

The majority of the simulations were highly significant after the calibration process, as we can observe by the presence of red asterisks in Figure 3. This means that the model can reproduce most of the trends of the data, underlying its reliability to make estimations. The statistical significance was performed using the Mann–Whitney U-test [24] and comparing the western blot protein data against the simulated levels, testing for a significant decrease and increase in protein levels. The same test will be used to assign significance to cell number and proliferation.

As we already discussed in Figure 1, we know that in the presence of E2, ER is bound and the production of cyclinD1 and c-Myc is amplified. In Figure 3 (a) we can observe the behavior of different proteins in the absence of E2. As we expected, the level of c-Myc decreases significantly over time, while only a small decrease is observed in the level of cyclinD1. The rapid decreases observed in c-Myc could be related to the sharp changes in E2 concentration in the medium, causing the cells to be blocked in the cycle phase G1, therefore decreasing the level of RB1-pp and decreasing the level of c-Myc. The increase in ER level doesn't need to startle us. From a fast

literature research, it is possible to understand that the half-life of the complex E2:ER is circa one hour smaller than the half-life of the not bound ER [25]. Therefore, the absence of E2 sort of stabilizes the ER and causes an increase in its levels. There are two main increases in ER value, and these correspond exactly to day 0 and day 3, the time steps at which the E2 depletion was performed by changing the medium of the cell culture.
The decrease in c-Myc levels causes the release of its inhibitor p21, as this can be observed in Figure 3 (a) (iv), even though, the data are noisy and cannot be considered significant.
As we already discussed, in the absence of E2, the cascade process that pilots the hyper-phosphorylation of RB1, creating RB1-pp, is not active. We can easily see from Figure 3 (a) (v) that the levels of RB1-pp decrease rapidly in the absence of E2.
Finally, we can observe a rapid decrease in the levels of free RB1. A main reason can be highlighted for this event, specifically, the decrease in free RB1 is connected to the decrease in proliferation, as the cells are blocked in the G1 phase and no free E2F is needed, therefore finding it linked to RB1, causing a lower level of free RB1. Also, several studies captured this behavior in response to E2 deprivation [26].
In Figure 3 (b) we can observe the behavior of different proteins in response to the treatment with ICI.
In the presence of ICI (Fulvestrant), the degradation of ER is activated, as we already observed in Figure 1.
The model can easily capture the decrease in ER levels given the presence of ICI, as we can observe from Figure 3 (b) (iii). The same can be seen for the other proteins, specifically, we can observe a significant reduction in the levels of all the proteins, similar to what we observed in the E2 deprivation.

4.1.1 Our data

Thanks to the available data we were able to reproduce the results shown under . Specifically, we used the initial parameters (without a refinement process) and we were able to obtain similar behaviors to the ones explained above, as we can see from Figure 4. Specifically, it is easy to observe that, the behavior of p21 is the same as what is already observed in Figure 3. Indeed, from Figure 4 (d) and (j), the simulation (in blue) has a quite different trend with respect to the experimental measures (in red). The same can be said for '-E2 total CyclinD1' (Figure 4 (b)).

4.2 Adding a new drug to the model requires limited new data

From the literature is known that, when adding a new variable in a mathematical model, like adding a new drug, the number of parameters that need to be re-calibrated varies depending on the level of detail and accuracy required by the model, meaning that it depends on the complexity and specificity of the mathematical model and the mechanism of action of the new drug [27].

In the context of this model, the research group explained to us that adding a new drug to the model requires only calibrating a few new parameters associated with the new drug. Furthermore, the researchers explain that it is only necessary to measure the response of only a few key proteins.
Specifically, in this case, the drug palbociclib was incorporated into the model, a drug that is clinically used in combination with endocrine therapy, as we explained in the introductory part of the report.

Palbociclib is an inhibitor of both CDK4 and CDK6-cyclinD1 kinase activity [13]. By inhibiting CDK4/6, palbociclib prevents the cell from exiting the G1 phase, leading to cell cycle arrest and reducing the levels of RB1-pp.

To calibrate the binding and unbinding parameters associated with palbociclib only two proteins were measured, specifically, c-Myc and RB1-pp, which are the main proteins affected by the presence of the drug.

In Figure 5 it is possible to observe the calibrated model when 1 μM of palbociclib is added to the medium. It is possible to observe that in the presence of the drug, the levels of RB1-pp and c-Myc decrease rapidly.

4.2.1 Our data

We can clearly see in Figure 6 that both c-Myc and RB1-pp decrease in the presence of palbociclib, as we expected. As above, a strong similarity with the researchers' simulation is observed.

4.3 The proliferation results can be explained by the RB1-pp level

As we previously saw, uncontrolled proliferation and cell growth is a hallmark of cancer. When dealing with treatments, proliferation is often used as a primary endpoint. With the term 'primary endpoint', we indicate a measure of efficiency and effectiveness of a treatment, meaning a measure that indicates if a specific outcome was achieved [28]. Since proliferation assays are easy to perform and various methods can be nowadays used, it is a commonly used technique to test the biological activity of a drug.

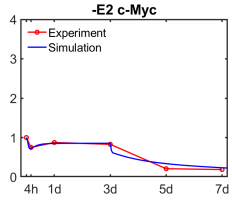

(a) *normalized c-Myc value*

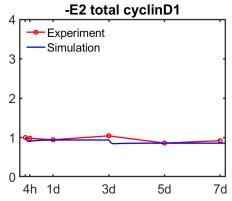

(b) *normalized total cyclinD1 value*

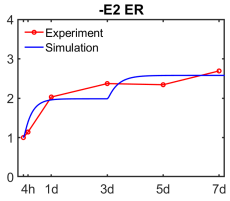

(c) *normalized ER value*

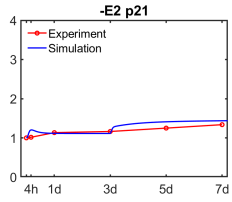

(d) normalized p21 value

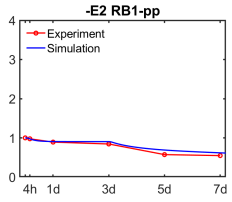

(e) normalized RB1-pp value

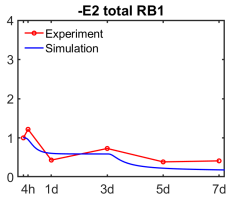

(f) normalized total RB1 value

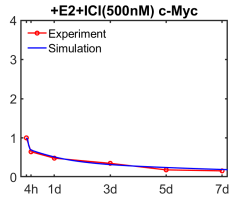

(g) *normalized c-Myc value*

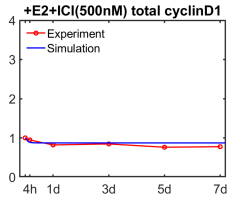

(h) *normalized total cyclinD1 value*

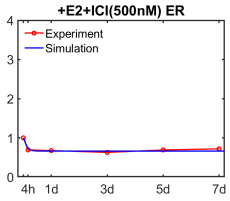

(i) *normalized ER value*

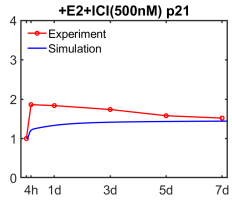

(j) normalized p21 value

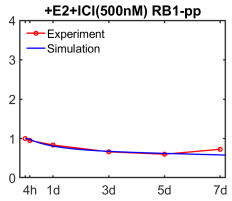

(k) normalized RB1-pp value

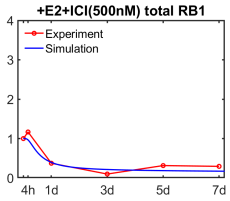

(l) normalized total RB1 value

Figure 4: Simulation vs experimental results from our implementation. Results of the protein levels in E2 deprivation (from (a) to (f)) and in the presence of ICI (from (g) to (l)).

This is important also in our case, the model needs to be able to keep track of the proliferation level, to define the efficiency of the treatments. The treatments we are considering in this research are all treatments that produce a G1 arrest, preventing the transition to the S phase by working on the phosphorylation level of RB1. Specifically, the research group explained to us that, in our model, we can assume that cell proliferation is controlled by the levels of RB1-pp. The proliferation rate is modeled as proportional to the number of current cells alive plus terms dealing with RB1-pp.

The formula that models cell proliferation is defined as follows:

$$\frac{dcell}{dt} = k_{pro} \times \left(1 + k_{proRB1pp} \times \frac{RB1pp^{p_{proRB1pp_2}}}{p_{proRB1pp_1}^{p_{proRB1pp_2}} + RB1pp^{p_{proRB1pp_2}}}\right) \times cells \times \left(1 - \frac{cell}{k_{carrying}}\right)$$

Figure 7 depicts cell proliferation levels in different conditions:

- Control condition: we can see that, as expected, in control conditions cell proliferation grows rapidly.
- E2 deprivation: the proliferation rate is smaller than the control condition. The results from the simulation are significant.
- ICI treatment: in this case, the proliferation rate is smaller than the one observed in the E2 deprivation condition.

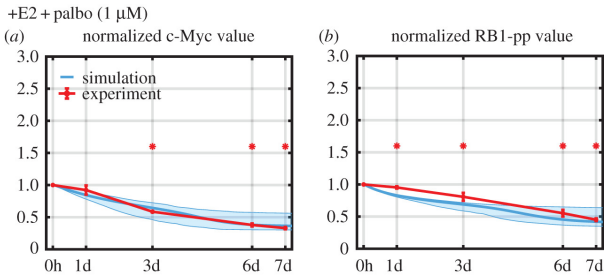

Figure 5: From [18]. Simulation and experimental results for protein-level changes in response to palbociclib. Simulations are shown in blue and experimental measurements are in red. Statistical significance is denoted by asterisks.

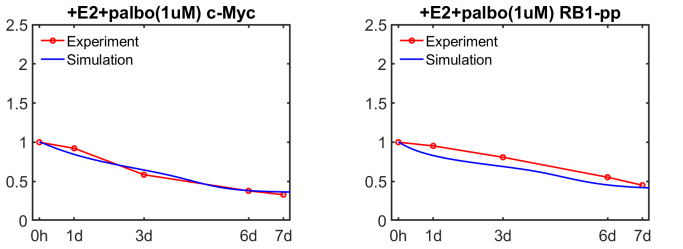

(a) *normalized c-Myc value* (b) *normalized total RB1-pp value*

Figure 6: Simulation and experimental results for protein-level changes in response to palbociclib. The experimental measures are marked in red, while the simulation results are marked in blue.

- Palbociclib treatment: in this last case, cell proliferation is comparable to the one observed when the culture is treated with ICI.

4.3.1 Our data

By retrieving the necessary data and implementing a function explaining the cell proliferation in our code, we were able to retrieve the plots shown in Figure 8. We can see that there is a high similarity between our results and the ones discussed above. Indeed, the simulation is able to describe accurately the experimental measures.

4.4 The model can predict the effect of combination treatments

The next step of the analysis is to test if the calibrated model is able to predict the effect of the combination of multiple therapies, which, as we know, is a common strategy to treat ER-positive breast cancer.

Specifically, the group initially focused on the effect of the combination of ICI and E2 deprivation, two endocrine therapies working at different levels to reduce the signaling activated by E2:ER.

We can see from Figure 9 that, as expected, a more relevant decrease in protein level is observed when the two treatments are used simultaneously. Indeed, the simulation results match significantly with the experimental ones, as can be observed by comparing the monotherapy experimental results (in cyan in the plot) and the simulation prediction (in blue in the plot). As already discussed, p21 and CyclinD1 are more noisy and the simulation isn't able to capture completely the behaviour of such proteins. The reason behind this could be related to the need for more parameters related to the equations explaining these protein changes. Moreover, we know that the model is based on assumptions that reduce the complexity and the mechanism of action of p21 and CyclinD1.

Figure 10 describes the effects of the combination of E2 deprivation and palbociclib on protein levels. We already discussed the importance of the combination of endocrine therapies and CDK6-cyclinD1 inhibitors. Indeed, palbociclib, by inhibiting Cdk4/6, prevents the cell from exiting the G1 phase, therefore blocking the proceeding of the cell cycle. Thanks to E2 deprivation, the level of estrogen is reduced, therefore slowing cancer growth. It is clear that the combination of these drugs works in a synergic way, by targeting E2:ER signaling at different levels.

From Figure 10 we can observe that the reduction in protein levels is greater than the one observed in monotherapies, as we already discussed in Figure 9. It is also possible to observe that there is an overall good agreement

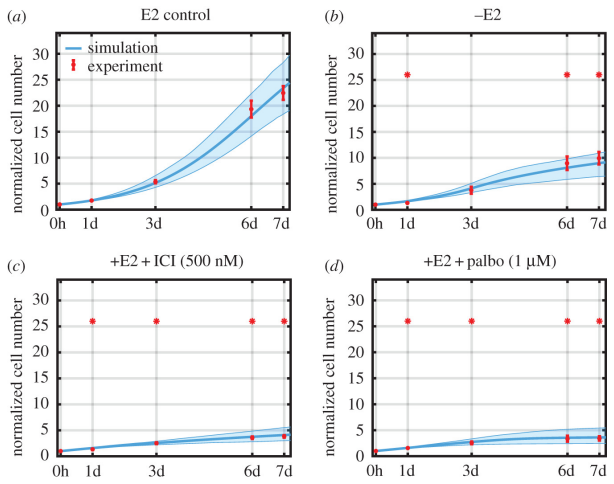

Figure 7: From [18]. Model simulations and experimental measurements of the normalized cell numbers under different treatment conditions. Experimental counts are in red and simulations are in cyan. ICI concentration is 500 nanoM, palbociclib concentration is 1 microM and E2 concentration is 10 nanoM. Statistically significant changes from the +E2 control are denoted by asterisks.

between the simulation prediction and the experimental level, even though, for RB1-pp the simulation is not completely concordant to the experimental measures at timesteps 6 days and 7 days. It is still important to notice that the decrease observed in RB1-pp when a combination treatment is applied is greater than the one observed when using monotherapies.

4.4.1 Our data

Regarding the ability of the model to predict the effect of combination treatments, we decided to work on the cell proliferation levels, investigating the efficiency of the treatments to block cancer progression.

Figure 11 depicts the proliferation levels in response to two treatments:

- Combination of E2 deprivation and ICI treatment.
- Combination of E2 deprivation and Palbociclib treatment.

We can observe that in the first case (Figure 11 (a)), the prediction is quite similar to the experimental results, plus, it is possible to observe, as we already saw in Figure 9, that the combination of these two therapies is more effective in slowing cell proliferation and, we can assume, cancer growth. The same can be observed in the second case (Figure 11 (b)), where, similarly to what was found in 10, the synergy of endocrine treatments and Cdk4/6 inhibitors is such to have a great response against cell proliferation.

4.5 Local sensitivity analysis of protein levels and proliferation

The local sensitivity analysis is a technique used to estimate the impact of variations in the input factor on the model's responses, indeed it gives an insight into the behavior of our mathematical model by investigating the impact of input parameters on the model's output. The sensitivity coefficient for a model output with respect to a specific parameter represents the percentage change in the model output divided by the percentage change in the parameter value. In mathematical terms, it can be expressed as:

$$SensitivityCoefficient = \frac{\Delta ModelOutput \backslash ModelOutput}{\Delta Parametervalue \backslash Parametervalue}$$

This coefficient helps quantify how variations in the parameter impact the overall model behavior.

Figure 12 represents the sensitivity coefficients of the most affected output of the model at day 7 as time points, which were identified as the cell proliferation, total RB1, and c-Myc, while the other proteins present low sensitivity.

By looking at the plots it is possible to see the cases for which the outputs of our model are most sensitive and also which parameters are most impactful :

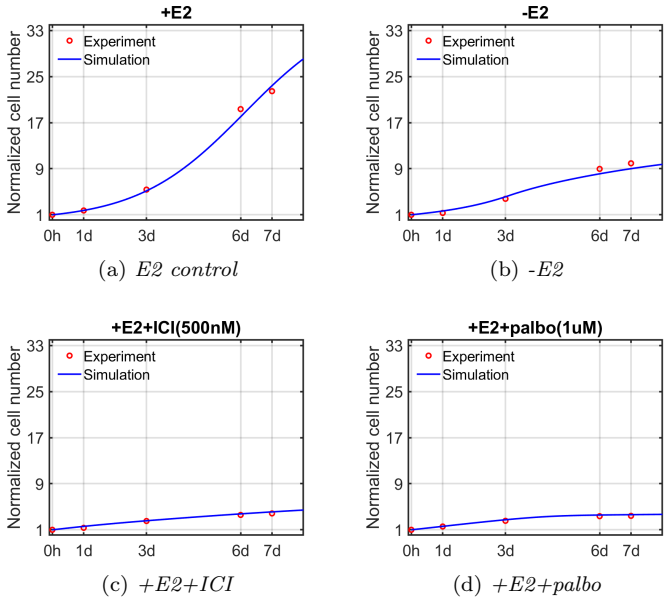

(a) *E2 control* (b) *-E2*

(c) *+E2+ICI* (d) *+E2+palbo*

Figure 8: Proliferation levels obtained from our implementation. The simulation results are depicted in blue, and the experiment measures are depicted in red.

- In the plot 12(a) the most significant sensitivity for c-Myc happened for +E2+ICI(500nM) treatment case and seems to affect the basal translation of cyclinE and p21(k_cyclinE and k_p21), also the phosphorylation of RB1-p is affected. These results are understandable, indeed the levels of c-Myc are affected by the parameters we just showed, which are confirmed by the biological model 1.
- For Total Rb1, 12(b), on the other hand, it seems that the -E2+ICI case is the most sensitive one, indeed the parameters that affect mostly are the ones involved with the basal transcription of cyclinE and c-Myc (parameters: k_cyclinE and k_cMyc). Also, parameters that represent the downregulation of p21 by c-Myc (p_p21cMyc_1), the phosphorylation of RB1-p by cyclinE (k_RB1pcyclinE), and the dephosphorylation of RB1-pp (p_RB1ppdepho_2) seem to be greatly involved. By observing the model 1 the sensitivity of these parameters is understandable, indeed all converge to affecting RB1-pp.
- In plot 12(c), which represents the cell number, it seems that the proliferation is most sensitive to both treatment cases with +E2+ICI and +E2+palbo(1μM). The greatest sensitivity values are associated with parameters that involve the transcription of cyclinE (k_cyclinE), the cyclinE phosphorylation of RB1-p (k_RB1pcyclineE), and basal transcription of p21 (k_p21)in the cases of palbociclib. These parameters are all associated with RB1-pp 1, which indeed is linked to cell proliferation.

4.6 The model can be used to explore the effect of sequential therapies

From the obtained results explained above, it is easy to understand that both monotherapies and combination therapies seem quite promising when dealing with breast cancer. In reality, these therapies can be applied only for a short time frame as resistance often arises thanks to cancer evolution [[29], [30]].

One possibility to address these mechanisms of resistance onset could be the alternation of various therapies. With that, the research group explained to us that a cycle of therapies is indicated, with the idea that in this way, the tumor proliferation is still targeted, but in a way that resistances are less prone to be generated since not only one level of signaling is targeted. This approach is already used in clinical research both in cancer studies [31] and bacteria ones [32].

Thanks to mathematical modeling, finding the right protocol to apply such therapy cycles is less complex with respect to what it could be from the clinical point of view. Given the large variation in dosing and timing that need to be selected for each treatment in the cycle, simulations are the only reliable technique to test such a number of possibilities.

Figure 13 (a) represents the changes in protein levels and proliferation for cells treated with palbociclib with or without a resistance mechanism while Figure 13 (b) represents the same proteins when cells are treated with

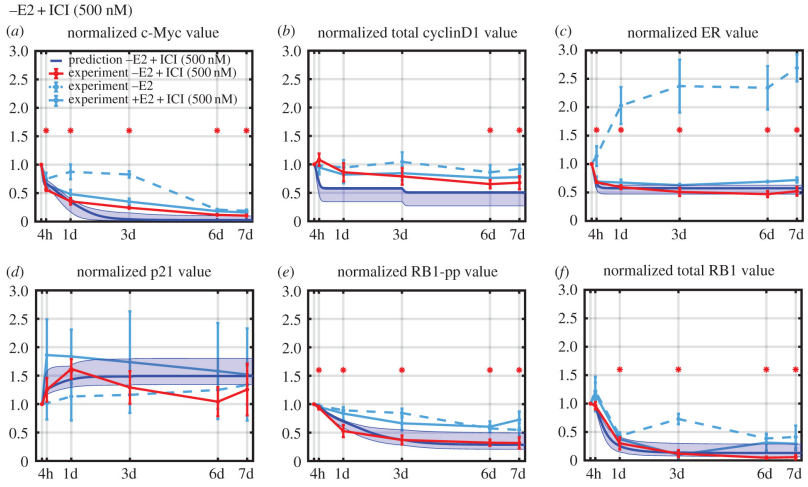

Figure 9: From [18]. Prediction simulations for protein-level changes in response to combination E2 deprivation +ICI therapy. ICI concentration is 500 nM. Experimental results are in red, simulations are in blue, and monotherapy experimental results are in cyan. Statistically significant changes are denoted by asterisks.

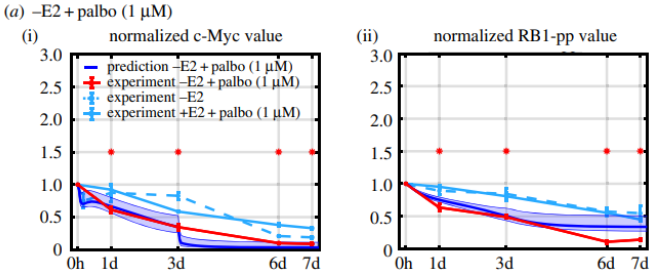

Figure 10: From [18]. Comparison of model predictions with experiment for combination therapies. Experimental data (red), simulations (blue) and monotherapy experimental results (cyan). (a) Prediction of c-Myc and RB1-pp levels in response to –E2 + palbociclib (1 micoM) combination treatment.

a cyclic therapy (alternating E2 deprivation and palbociclib) or with a monotherapy (palbociclib), taking also in consideration mechanisms of resistance. Figure 13 (c) is the same as (b), the only difference is that the cycle therapy alternates ICI and palbociclib.

As discussed above, in the presence of mechanisms of resistance onset, both monotherapies and combined therapies' efficiency and effect are lost, as we can observe from Figure 13 (a). Indeed, an initial effect of the therapy is observed (in purple, till day ~ 30 for cell proliferation, till day ~ 10 for CyclinD1 and RB1-pp) but, as soon as resistance is obtained by the cells, the therapy is no longer effective.

When dealing with cyclic therapies, different behavior is observed. Indeed, in Figure 13 (b) and (c), it is possible to observe that, thanks to the alteration of drugs, the time required to observe a slight difference in the effect of the treatment is circa three times greater than the one observed for monotherapies. It is still important to notice that at the end of the simulation, even when applying cyclic treatments, a sort of mechanism of resistance seems to take place, given the decrease in effect in maintaining stable cell proliferation and protein levels.

It is also important to notice that between cases (b) and (c) no major differences are notable, indeed, in both cases, endocrine therapy is associated with palbociclib. This could mean that there are no major reasons to choose one endocrine therapy over the other when looking only at the overall effect.

5 Discussion

This study focuses on ER-positive breast cancer, creating a mathematical model able to describe the aberrant ER signaling that takes place in these cancer cells. The model captures the main key proteins that regulate the ER signaling that are activated by it, some assumptions are taken to create a not-to-complex model. The model calibration was performed by using sets of parameters derived from experimental data and applying a process of parameter estimation via the usage of a genetic algorithm.

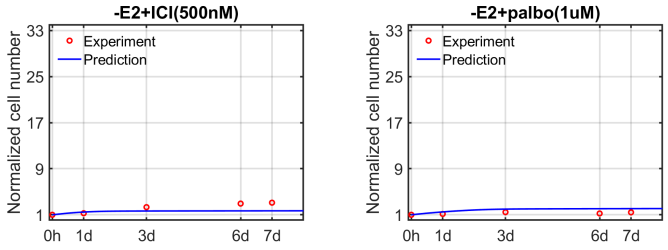

(a) *-E2+ICI* (b) *-E2+Palbo*

Figure 11: Proliferation levels obtained from our implementation. The simulation results are depicted in blue, and the experiment measures are depicted in red.

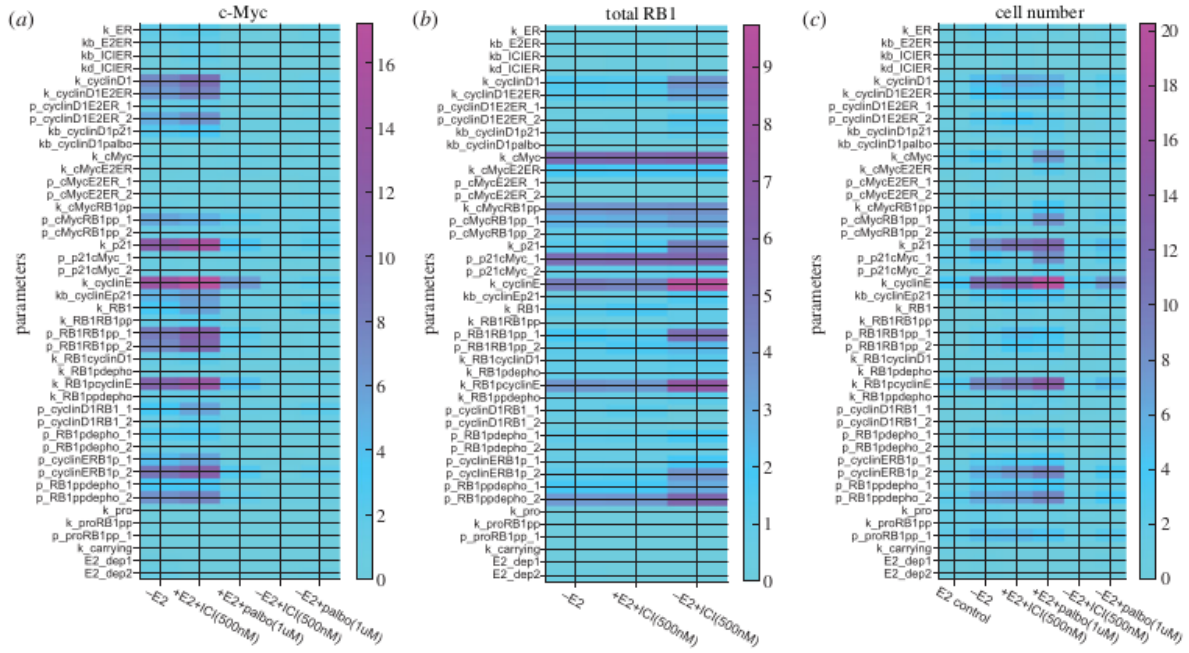

Figure 12: From [18].Local sensitivity analysis of the effect on c-Myc level, total RB1 level, and cell number of each model parameter. Each of the parameters is changed by ±5% and the sensitivity at day 7 for each treatment is plotted.

The model was found to be predictive for cell proliferation and protein levels regulating ER signaling, both in terms of monotherapies and combined therapies. Also, a key aspect related to the model construction is that, given the level of complexity and specificity required, the addition of a new drug to the model required only some minor adjustments with the addition of parameters strictly related to the mechanism of action of the given drug.

Despite the model's simplicity with respect to the complexity of the biological system of cancer cells, we were able to observe that it is possible to make assumptions on the predictive ability of the model regarding the utilization of cycle therapies in the context of resistance onset. This represents a great instance of the power of such models, indeed, experimentally the study of such matter would be impracticable, given the high number of possibilities for the different drug dosages and timesteps.

5.0.1 Conclusion of this report

Our re-implementations of the model returned very similar results to the one found in the paper, even though not all plots were re-created, but only a portion of them. This project provided us the possibility to have a more in-depth understanding of the matter of mathematical model generation, model precision, and accuracy. We also were able to improve our programming skills and problem-solving skills, since we decided to implement our code in MATLAB, a language we are still learning.

Finally, as future prospects, we think that it could be interesting to analyze the modeling using a stochastic

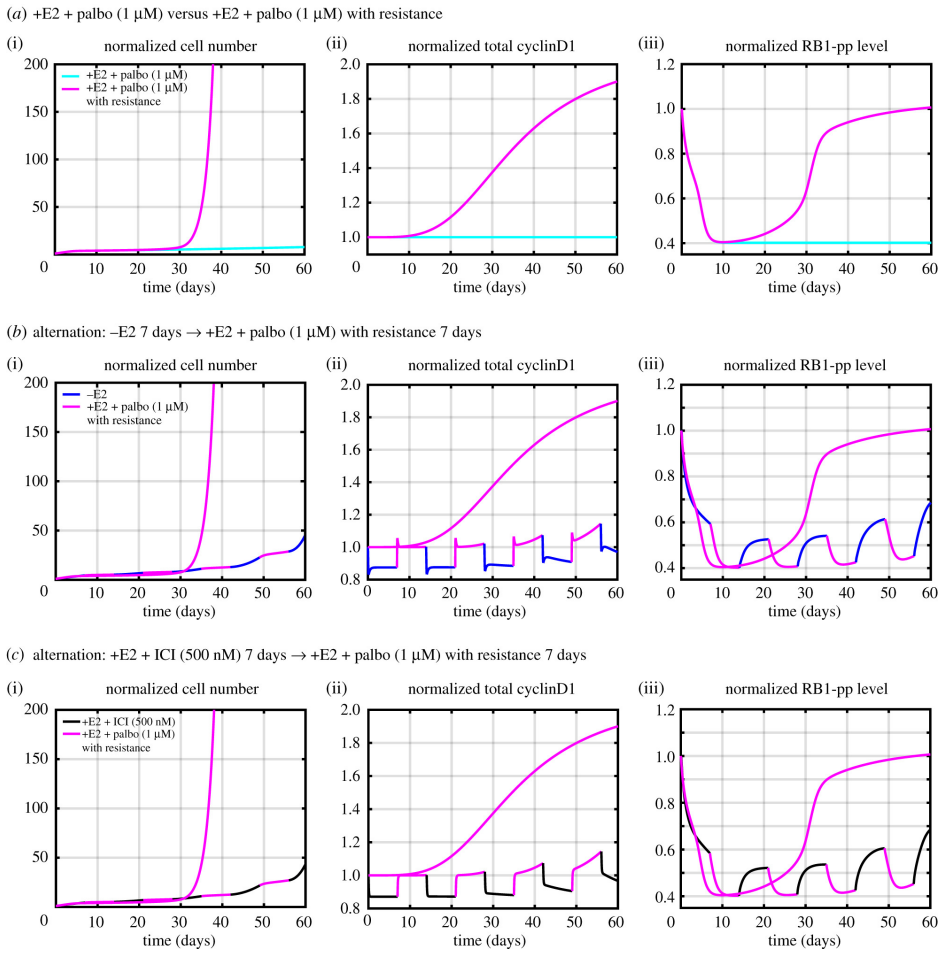

Figure 13: From [18]. Model simulations of possible alternating therapies compared with continuous monotherapy with an added resistance mechanism. (a) Continuous palbociclib therapy with and without the resistance mechanism are compared. (b) Continuous palbociclib therapy is compared with alternation of E2 deprivation and palbociclib therapies. (c) Continuous palbociclib therapy is compared with an alternation of ICI and palbociclib therapies. Doses: E2 (10 nM), ICI (500 nM), palbociclib (1 microM). The simulations use the lowest cost parameter set, and all simulations in (b) and (c) include the resistance mechanism.

simulation since these are more appropriate when a system is less known and a degree of uncertainty in input, output or both are needed. Indeed, when dealing with cancer cells, treatments, and drug resistance, a certain degree of uncertainty is needed since the mechanisms regulating such signaling are not completely known and a degree of uncertainty is always present when dealing with biological systems.

6 Appendix - A

The code and additional information can be found inside the GitHub repository.

7 Appendix - B

Abbreviations/Model variable description:

ER: Estrogen receptor
E2ER: Estrogen bound estrogen receptor
ICIER: ICI 182,780 bound estrogen receptor
cyclinD1: Protein cyclinD1
cyclinD1p21: p21 bound cyclinD1 protein
cyclinD1palbo: palbociclib bound cyclinD1 protein
cMyc: Protein c-Myc
p21: Protein p21
cyclinE: Protein cyclinE
cyclinEp21: p21 bound cyclinE protein
RB1: Retinoblastoma protein
RB1p: Hypophosphorylated RB1
RB1pp: Hyperphosphorylated RB1
cell: Cell number

Model parameter description

k_{ER}	Translation rate of ERα
kd_{ER}	Degradation rate of ERα
kd_{E2ER}	Degradation rate of E2ER
kb_{E2ER}	Binding rate between E2 and ERα
kub_{E2ER}	Unbinding rate between E2 and ERα
kb_{ICIER}	Binding rate between ICI and ERα
kub_{ICIER}	Unbinding rate between ICI and ERα
kd_{ICIER}	Degradation rate of ICIER
$k_{cyclinD1}$	Translation rate of cyclinD1
$kd_{cyclinD1}$	Degradation rate of cyclinD1
$k_{cyclinD1E2ER}$	Increased cyclinD1 translation by E2ER
$p_{cyclinD1E2ER_1}$	Parameter 1 of cyclinD1 increased translation by E2ER
$p_{cyclinD1E2ER_2}$	Parameter 2 of cyclinD1 increased translation by E2ER
$kb_{cyclinD1p21}$	Binding rate between cyclinD1 and p21
$kub_{cyclinD1p21}$	Unbinding rate between cyclinD1 and p21
$kb_{cyclinD1palbo}$	Binding rate between cyclinD1 and palbociclib
$kub_{cyclinD1palbo}$	Unbinding rate between cyclinD1 and palbociclib
k_{cMyc}	Translation rate of c-Myc
kd_{cMyc}	Degradation rate of c-Myc
$k_{cMycE2ER}$	Increased translation of c-Myc by E2ER
$p_{cMycE2ER_1}$	Parameter 1 of c-Myc increased translation by E2ER
$p_{cMycE2ER_2}$	Parameter 2 of c-Myc increased translation by E2ER
$k_{cMycRB1pp}$	Increased translation of c-Myc by RB1-pp
$p_{cMycRB1pp_1}$	Parameter 1 of c-Myc increased translation by RB1-pp
$_{cMycRB1pp_2}$	Parameter 2 of c-Myc increased translation by RB1-pp
k_{p21}	Translation rate of p21
kd_{p21}	Degradation rate of p21
$p_{p21cMyc_1}$	Parameter 1 of p21 inhibited translation by c-Myc
$p_{p21cMyc_2}$	Parameter 2 of p21 inhibited translation by c-Myc
$k_{cyclinE}$	Translation rate of cyclinE

$kd_{cyclinE}$	Degradation rate of cyclinE
$kb_{cyclinEp21}$	Binding rate between cyclinE and p21
$kub_{cyclinEp21}$	Unbinding rate between cyclinE and p21
k_{RB1}	Translation rate of RB1
kd_{RB1}	Degradation rate of RB1
$k_{RB1RB1pp}$	Increased RB1 translation by RB1-pp
$p_{RB1RB1pp_1}$	Parameter 1 of RB1 increased translation by RB1-pp
$p_{RB1RB1pp_2}$	Parameter 2 of RB1 increased translation by RB1-pp
$k_{RB1cyclinD1}$	Phosphorylation rate of RB1 by cyclinD1
$k_{RB1pdepho}$	Dephosphorylation rate of RB1-p
kd_{RB1p}	Degradation rate of RB1-p
$k_{RB1pcyclinE}$	Phosphorylation rate of RB1-p by cyclinE
$k_{RB1pphepho}$	Dephosphorylation rate of RB1-pp
kd_{RB1pp}	Degradation rate of RB1-pp
$p_{cyclinD1RB1_1}$	Parameter 1 of RB1 phosphorylation by cyclinD1
$p_{cyclinD1RB1_2}$	Parameter 2 of RB1 phosphorylation by cyclinD1
$p_{RB1pdepho_1}$	Parameter 1 of RB1-p dephosphorylation
$p_{RB1pdepho_2}$	Parameter 2 of RB1-p dephosphorylation
$p_{cyclinERB1p_1}$	Parameter 1 of RB1-p phosphorylation by cyclinE
$p_{cyclinERB1p_2}$	Parameter 2 of RB1-p phosphorylation by cyclinE
$p_{RB1ppdepho_1}$	Parameter 1 of RB1-pp dephosphorylation
$p_{RB1ppdepho_2}$	Parameter 2 of RB1-pp dephosphorylation
k_{pro}	Basal proliferation rate
$k_{proRB1pp}$	Proliferation rate increased by RB1-pp
$p_{proRB1pp_1}$	Parameter 1 of proliferation rate increased by RB1-pp
$p_{proRB1pp_2}$	Parameter 2 of proliferation rate increased by RB1-pp
$k_{carrying}$	Carrying capacity
$E2_{dep_1}$	Estrogen concentration in E2 deprivation media 0 to 3days
$E2_{dep_2}$	Estrogen concentration in E2 deprivation media 3 to 7days
$E2$	Estrogen concentration
ICI	ICI 182,780 concentration
$palbo$	Palbociclib concentration

8 Appendix - C

Reactions (Avogadro's number is $N_A = 6.022 \cdot 10^2 3$, Cell MCF-7 volume is $V = 1.79 \cdot 10^{-9}$) :

1. $\emptyset \xrightarrow{c_{ER}}$ ER Zero-order reaction $c_{ER} = k_{ER} \cdot (N_A \cdot V)$
2. ER $\xrightarrow{cd_{ER}} \emptyset$ Zero-order reaction $cd_{ER} = kd_{ER} \cdot (N_A \cdot V)$
3. ER + E_2 $\xrightarrow{cb_{E2ER}}$ E_2ER Second-order reaction $cb_{E2ER} = \frac{kb_{E2ER}}{(N_A \cdot V)}$
4. ER + ICI $\xrightarrow{cb_{ICIER}}$ ERICI Second-order reaction $cb_{ICIER} = \frac{kb_{ICIER}}{(N_A \cdot V)}$
5. E_2ER $\xrightarrow{cub_{E2ER}}$ E_2 + ER Second-order reaction $cub_{E2ER} = \frac{kub_{E2ER}}{(N_A \cdot V)}$
6. E_2ER $\xrightarrow{cd_{E2ER}} \emptyset$ Zero-order reaction $cd_{E2ER} = kd_{E2ER} \cdot (N_A \cdot V)$
7. ICIER $\xrightarrow{cub_{ICIER}}$ ER + ICI Second-order reaction $cub_{ICIER} = \frac{kub_{ICIER}}{(N_A \cdot V)}$
8. ICIER $\xrightarrow{cd_{ICIER}} \emptyset$ Zero-order reaction $cd_{ICIER} = kd_{ICIER} \cdot (N_A \cdot V)$
9. cycD $\xrightarrow{cd_{cycD}} \emptyset$ Zero-order reaction $cd_{cycD} = kd_{cycD} \cdot (N_A \cdot V)$
10. $\emptyset \xrightarrow{c_{cycD} + c_{cycDE2ER}}$ cycD Zero-order reaction $c_{cycD} + c_{cycDE2ER} = [k_{cycD} \cdot (N_A \cdot V)] + [k_{cycDE2ER} \cdot (N_A \cdot V)]$

11. $\text{cycD} + \text{p}_{21} \xrightarrow{cb_{cycDp21}} \text{cycDp}_{21}$ Second-order reaction $cb_{cycDp21} = \frac{kb_{cycDp21}}{(N_A \cdot V)}$

12. $\text{cycD} + \text{palbo} \xrightarrow{cb_{cycDpalbo}} \text{cycDpalbo}$ Second-order reaction $cb_{cycDpalbo} = \frac{kb_{cycDpalbo}}{(N_A \cdot V)}$

13. $\text{cycDp}_{21} \xrightarrow{cub_{cycDp21}} \text{cycD} + \text{p}_{21}$ Second-order reaction $cub_{cycDp21} = \frac{kub_{cycDp21}}{(N_A \cdot V)}$

14. $\text{cycDp}_{21} \xrightarrow{cd_{cycDp21}} \emptyset$ Zero-order reaction $cd_{cycDp21} = kd_{cycDp21} \cdot (N_A \cdot V)$

15. $\text{cycDpalbo} \xrightarrow{cd_{cycDpalbo}} \emptyset$ Zero-order reaction $cd_{cycDpalbo} = kd_{cycDpalbo} \cdot (N_A \cdot V)$

16. $\text{cycDpalbo} \xrightarrow{cub_{cycDpalbo}} \text{cycD} + \text{palbo}$ Second-order reaction $cub_{cycDpalbo} = \frac{kub_{cycDpalbo}}{(N_A \cdot V)}$

17. $\text{myc} \xrightarrow{cd_{myc}} \emptyset$ Zero-order reaction $cd_{myc} = kd_{myc} \cdot (N_A \cdot V)$

18. $\emptyset \xrightarrow{c_{myc} + c_{E2ERmyc} + c_{mycRB1pp}} \text{myc}$ Zero-order reaction $c_{myc} + c_{E2ERmyc} + c_{mycRB1pp} = [k_{myc} \cdot (N_A \cdot V)] + [k_{E2ERmyc} \cdot (N_A \cdot V)] + [k_{mycRB1pp} \cdot (N_A \cdot V)]$

19. $\text{p}_{21} \xrightarrow{cd_{p21}} \emptyset$ Zero-order reaction $cd_{p21} = kd_{p21} \cdot (N_A \cdot V)$

20. $\emptyset \xrightarrow{c_{p21} - c_{mycp21}} \text{p}_{21}$ Zero-order reaction $c_{p21} - c_{mycp21} = [k_{p21} \cdot (N_A \cdot V)] - [k_{mycp21} \cdot (N_A \cdot V)]$

21. $\text{cycE} \xrightarrow{cd_{cycE}} \emptyset$ Zero-order reaction $cd_{cycE} = kd_{cycE} \cdot (N_A \cdot V)$

22. $\emptyset \xrightarrow{c_{cycE}} \text{cycE}$ Zero-order reaction $c_{cycE} = k_{cycE} \cdot (N_A \cdot V)$

23. $\text{cycE} + \text{p}_{21} \xrightarrow{cb_{cycEp21}} \text{cycEp}_{21}$ Second-order reaction $cb_{cycEp21} = \frac{kb_{cycEp21}}{(N_A \cdot V)}$

24. $\text{cycEp}_{21} \xrightarrow{cub_{cycEp21}} \text{cycE} + \text{p}_{21}$ Second-order reaction $cub_{cycEp21} = \frac{kub_{cycEp21}}{(N_A \cdot V)}$

25. $\text{cycEp}_{21} \xrightarrow{cd_{cycEp21}} \emptyset$ Zero-order reaction $cd_{cycE} = kd_{cycE} \cdot (N_A \cdot V)$

26. $\text{RB}_1 \xrightarrow{cd_{RB1}} \emptyset$ Zero-order reaction $cd_{RB1} = kd_{RB1} \cdot (N_A \cdot V)$

27. $\emptyset \xrightarrow{c_{RB1} + c_{RB1-RB1pp}} \text{RB}_1$ Zero-order reaction $c_{RB1} + c_{RB1RB1pp} = [k_{RB1} \cdot (N_A \cdot V)] + [k_{RB1RB1pp} \cdot (N_A \cdot V)]$

28. $\text{RB}_1 + \text{cycD} \xrightarrow{c_{RB1cycD}} \text{RB}_1\text{p}$ Second-order reaction $cb_{RB1cycD} = \frac{kb_{RB1cycD}}{(N_A \cdot V)}$

29. $\text{RB}_1\text{p} \xrightarrow{c_{RB1pdepho}} \text{RB}_1$ First-order reaction $c_{RB1pdepho} = k_{RB1pdepho}$

30. $\text{RB}_1\text{p} \xrightarrow{cd_{RB1p}} \emptyset$ Zero-order reaction $cd_{RB1p} = kd_{RB1p} \cdot (N_A \cdot V)$

31. $\text{RB}_1\text{p} + \text{cycD} \xrightarrow{c_{RB1pcycD}} \text{RB}_1\text{p}$ Second-order reaction $cb_{RB1pcycD} = \frac{kb_{RB1pcycD}}{(N_A \cdot V)}$

32. $\text{RB}_1\text{pp} \xrightarrow{c_{RB1ppdepho}} \text{RB}_1\text{p}$ First-order reaction $c_{RB1ppdepho} = k_{RB1ppdepho}$

33. $\text{RB}_1\text{pp} \xrightarrow{cd_{RB1pp}} \emptyset$ Zero-order reaction $cd_{RB1pp} = kd_{RB1pp} \cdot (N_A \cdot V)$

In figure 14 we can observe the stochastic simulation results. We specifically decided to show only the levels of the protein c-Myc, since it is clearly observable that the stochastic simulation has a strange behavior and the levels of c-Myc are not comparable with the one of the deterministic simulation, nor the original paper results. We indeed think that two major reasons for this strange behavior can be highlighted:

- The conversion of the ODE into reactions could be wrong. Indeed, the majority of the ODEs are simple and easy to transform but a couple of them are complex and the erroneous conversion could cost us the simulation.
- The conversion of the deterministic rates to stochastic ones could be wrong.

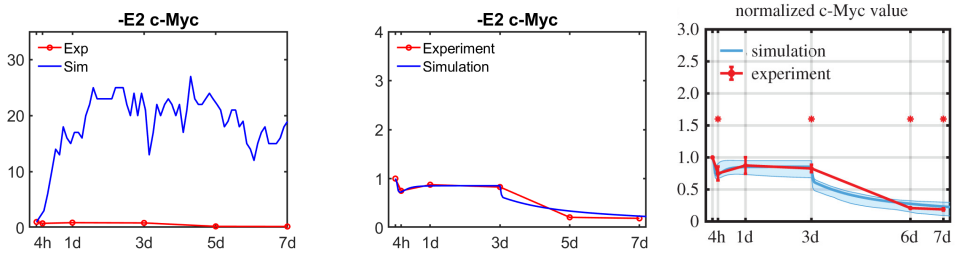

(a) *Stochastic simulation* (b) *Deterministic simulation* (c) *Original paper*

Figure 14: Comparison between the results of the stochastic simulation, the deterministic simulation, and the original paper in terms of the levels of the proteins c-Myc.

References

1. Smolarz B, e. a. Breast Cancer-Epidemiology, Classification, Pathogenesis and Treatment (Review of Literature). *Cancers (Basel).* (2022).
2. Koh J, K. M. Introduction of a New Staging System of Breast Cancer for Radiologists: An Emphasis on the Prognostic Stage. *Korean J Radiol.* (2019).
3. Et al, J. C. PAM50 Intrinsic Subtype Profiles in Primary and Metastatic Breast Cancer Show a Significant Shift toward More Aggressive Subtypes with Prognostic Implications. *Cancers (Basel).* (2021).
4. Yersal O, B. S. Biological subtypes of breast cancer: Prognostic and therapeutic implications. *World J Clin Oncol* (2014).
5. Et al., B. F. Cancer Incidence in Five Continents: Inclusion criteria, highlights from Volume X and the global status of cancer registration. *Int J Cancer.* (2015).
6. Et al., P. C. Molecular portraits of human breast tumours. *Nature.* (2000).
7. Et al., H. N. Breast cancer. *Nat Rev Dis Primer.* (2019).
8. Et al., R. J. Racial/ethnic differences in the outcomes of patients with metastatic breast cancer: contributions of demographic, socioeconomic, tumor and metastatic characteristics. *Breast Cancer Res Treat.* (2019).
9. Et al., K. B. Annual Report to the Nation on the Status of Cancer, 1975- 2011, Featuring Incidence of Breast Cancer Subtypes by Race/Ethnicity, Poverty, and State. *JNCI J Natl Cancer Inst.* (2015).
10. Shiovitz S, K. L. Genetics of breast cancer: a topic in evolution. *Ann Oncol.* (2015).
11. Et al., C. G. H. F. B. C. Familial breast cancer: collaborative reanalysis of individual data from 52 epidemiological studies including 58,209 women with breast cancer and 101,986 women without the disease. *Lancet Lond Engl.* (2001).
12. Goel S Bergholz JS, Z. J. Targeting CDK4 and CDK6 in cancer. *Nat Rev Cancer* (2022).
13. Cadoo KA Gucalp A, T. T. Palbociclib: an evidence-based review of its potential in the treatment of breast cancer. *Breast Cancer (Dove Med Press)* (2014).
14. Et al., E. J. A Review of Endocrine Therapy in Early-stage Breast Cancer: The Journey From Crudeness to Precision. *Am J Clin Oncol.* (2023).
15. Clinical data. Br J Cancer., R. J. ICI 182,780 (Fulvestrant), the first oestrogen receptor downregulator, current clinical data. *Br J Cancer* (2001).
16. Et al, R. R. Systematic review of aromatase inhibitors in the first line treatment for hormone sensitive advanced or metastatic breast cancer. *Breast Cancer Res Treat* (2010).
17. Camarillo, I. G. *et al.* in (Woodhead Publishing, 2014).
18. Et al, H. W. Mathematical modeling of breast cancer cells in response to endocrine therapy and Cdk4/6 inhibition. *R. Soc. Interface* (2020).
19. FI, M. & F, D. A. Cyclin D1 in Cancer: A Molecular Connection for Cell Cycle Control, Adhesion and Invasion in Tumor and Stroma. *Cells* (2020).
20. K, M. D. T. S. I. A. M. D. S. c-Myc and cancer metabolism. *Clin Cancer Res* (2012).

21. in. *Bone Sarcomas and Bone Metastases - From Bench to Bedside (Third Edition)* (ed Heymann, D.) Third Edition (Academic Press, 2022).

22. BH, A. A. P. P21 and p27: roles in carcinogenesis and drug resistance. *Expert Rev Mol Med* (2008).

23. François Fages Steven Gay, S. S. Inferring reaction systems from ordinary differential equations. *Theoretical Computer Science* (2015).

24. Patrick E. McKnight, J. N. Mann-Whitney U Test. *The Corsini Encyclopedia of Psychology* (2010).

25. Et al, B. M. Estrogenic and antiestrogenic regulation of the half-life of covalently labeled estrogen receptor in MCF-7 breast cancer cells. *J Steroid Biochem Mol Biol* (1996).

26. Et al, C. J. A pure estrogen antagonist inhibits cyclin E-Cdk2 activity in MCF-7 breast cancer cells and induces accumulation of p130-E2F4 complexes characteristic of quiescence. *J. Biol. Chem* (2000).

27. Et al., A. Z. Numerical solution of a new mathematical model for intravenous drug administration. *Evol. Intel* (2023).

28. Et al., A. D. L. Integrating Molecular Biomarker Inputs Into Development and Use of Clinical Cancer Therapeutics. *Front. Pharmacol.* (2021).

29. Et al., A. D. H. Endocrine-Resistant Breast Cancer: Mechanisms and Treatment. *Breast Care* (2020).

30. Et al., F. H. Z. CDK4/6 inhibitor resistance in estrogen receptor positive breast cancer, a 2023 perspective. *Front. Cell Dev Biol.* (2023).

31. Et al., J. F. Evolution of Resistance to Targeted Anti-Cancer Therapies during Continuous and Pulsed Administration Strategies. *PLoS Computational Biology* (2009).

32. Et al., D. N. Steering Evolution with Sequential Therapy to Prevent the Emergence of Bacterial Antibiotic Resistance. *PLos Comput Biol.* (2015).